Chemical Engineering Journal 380 (2020) 122375

Contents lists available at ScienceDirect

Chemical Engineering Journal

journal homepage: www.elsevier.com/locate/cej

# Modified biochar for phosphate adsorption in environmentally relevant conditions

Yimin Huang[a,b,c], Xinqing Lee[a,*], Matteo Grattieri[c], Mengwei Yuan[c], Rong Cai[c], Florika C. Macazo[c], Shelley D. Minteer[c,*]

[a] State Key Laboratory of Environmental Geochemistry, Institute of Geochemistry, Chinese Academy of Science, Guiyang, Guizhou 550081, China
[b] University of Chinese Academy of Sciences, Beijing 100049, China
[c] Departments of Chemistry and Materials Science & Engineering, University of Utah, 315 S 1400 E, Salt Lake City, UT 84112, United States

## HIGHLIGHTS

- Highly efficient phosphorus removal over a wide pH range.
- Adsorption properties of different materials evaluated by partition coefficient.
- Excellent adsorption performance at low phosphate concentrations.

## GRAPHICAL ABSTRACT

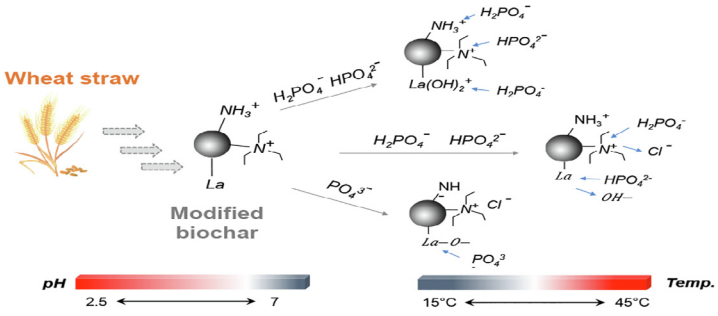


## ARTICLE INFO

*Keywords:*
Wheat straw biochar
Phosphate removal
Quaternary chitosan
Lanthanum
Partition coefficient

## ABSTRACT

Herein, we explored the modification of wheat straw biochar with chitosan, quaternary ammonium salt, and lanthanum for enhanced phosphate removal in environmentally relevant conditions. Specifically, a new amine protected cross-linking method was utilized to modify the absorbent material for maximum adsorption capacity, reaching 109 ± 4 mg P $g^{-1}$. The high phosphate removal performance of the composite was not significantly affected in a broad range of temperature (15–45 °C) and pH (2.5–7). 30 min allowed reaching a 100% adsorption equilibrium for 100 mg P $L^{-1}$, and 93% for 25 mg P $L^{-1}$, thus, significantly reducing the treatment time compared to previous reports. The highest partition coefficient 172.1 mg $g^{-1}$ $\mu M^{-1}$ was obtained at a concentration of 25 mg $L^{-1}$, and the phosphorus removal rate was as high as 99.98%, indicating La/GTB have great adsorption performance at low phosphate concentration. The adsorption mechanisms of the composite are extensively described, where electrostatic interaction, ligand exchange, and Lewis acid-base interaction contribute to the process. All of the above-mentioned advantages make the prepared composite of great interest for the development of materials for on-site phosphate removal.

## 1. Introduction

Phosphorus (P) is an essential nutrient for plant growth and development. However, excessive fertilization in agriculture and the resulted runoff of P [1] has led to increasing problems of eutrophication in many aquatic environments [2]. Various techniques have been studied to deal with this issue, including biological processes, chemical precipitation, ion exchange, and adsorption [3,4]. The latter can be

* Corresponding authors.
*E-mail addresses:* lee@mail.gyig.ac.cn (X. Lee), minteer@chem.utah.edu (S.D. Minteer).

https://doi.org/10.1016/j.cej.2019.122375
Received 26 June 2019; Received in revised form 28 July 2019; Accepted 29 July 2019
Available online 05 August 2019
1385-8947/ 

considered as the most attractive approach due to its operational simplicity, high effectiveness, low cost, and, most importantly, the availability of a wide range of adsorbents [5]. Previous reports of adsorbents effectively removing phosphate include aluminum oxide, ferric hydroxide, calcium hydroxide, and chitosan. However, iron-based adsorbents are sensitive to changes in redox conditions, and iron-bound phosphates are released when reducing conditions exist on the surface of the deposit. In addition, phosphate-removing efficiency of the Fe-containing material is lowered at high pH conditions, and the bound phosphorus may be desorbed by OH. In contrast to ferrous materials, the surface precipitation of the phosphate by the Ca-based material at high pH can be promoted, but the low pH hinders the precipitation of phosphorus on its surface. Finally, when the phosphate concentration is relatively low, the process is usually less effective [5]. Conversely, adsorbent modified by chitosan show high phosphate adsorption only in low pH solution [6]. The presented issues motivated studies on the synthesis of novel materials with high phosphate removal capacity at both acidic and basic conditions.

Quaternary chitosan can effectively absorb anion at both acidic and basic conditions due to its strong basic nature [6]; however, it cannot be directly used as adsorbent because of its poor mechanical strength and difficult separation from water. This disadvantage can be resolved by combining the quaternary chitosan with a host material, such as biochar. However, chitosan solubility at acidic solution required the use of a cross-linking agent before application as adsorbent [7], and cross-linking is prone to occur on the amine group instead of the hydroxyl group, weakening the adsorption capacity of the composite and making the process challenging [8–11]. Accordingly, efforts have been made to process the adsorbent with formaldehyde [8], or benzaldehyde [12], before performing the cross-linking reaction, to then release the protected amino groups through reaction with HCl solution. Many studies reported that the adsorption capacity of the adsorbent was significantly improved by following this new cross-linking method [11–13]. However, the efficiency may be overestimated due to the unreasonable comparison between the two cross-linking methods, requiring a better elucidation of the two approaches, to better define and select the best experimental procedure.

Similarly to quaternary chitosan, lanthanum (La) is an efficient adsorbent of phosphate at a wide range of pH, particularly at low phosphate concentrations [5]. Compared to other rare earth elements, La is environmentally friendly, cost-effective, and insensitive to redox conditions [5,14,15,4]. Once reacted with phosphate, the latter is hardly released due to the *Ksp* of the lanthanum–phosphate complexes in aqueous solution and seawater ($-24.76$ and $-27.92$) [14], which is advantageous for the removal of P from water. Moreover, the sorption efficiency can be further enhanced by diffusing La into activated carbon fiber or mesoporous silicate materials [16], which fixes La into the structure [4], as well as facilitates its homogeneous distribution in a large surface area or abundant pores [15]. Despite these advantages, the activated carbon fibers or mesoporous silicate materials are too expensive for application in the field. With the aim of developing a more cost-effective system, alternative material should be tested [15]. Biochar is a potential alternative for its low cost, large surface area, and abundant pores. Especially, > 80 million tons of wheat straw are produced all over the world [17], which are usually burned by the farmers to avoid interference of the straw left in the field with tillage and seeding [18]. Accordingly, utilization of straw derived biochar can prevent waste of resources and atmospheric pollution resulting from the burning process. In this study, we used wheat straw biochar as a sustainable supporting material, and modified it with quaternary-ammonium-processed chitosan and lanthanum hydroxide to improve phosphate adsorption at a wide range of pH, to achieve effective phosphate removal in environmentally relevant conditions. Four main steps can be identified as follows: (1) quaternary ammonium chitosan load on biochar, using two cross-linking methods (direct cross-linking and indirect cross-linking method) and comprehensive efficacy evaluation of new the cross-linking method. (2) Selection of the composite having the highest phosphorus adsorption capacity for the following lanthanum loading. (3) Study of the effects of various experimental conditions on the ability of the finished composite to adsorb phosphorus, such as pH, temperature, and time. (4) Finally, the maximum phosphorus adsorption capacity, partition coefficient, and adsorption mechanism of the composite were investigated.

## 2. Materials and methods

### 2.1. Chemicals and materials

Biochar was produced from wheat straw as specified in the following section. Chitosan (CS, MW: 310–375 kDa), glutaraldehyde solution (25% wt. % in $H_2O$), glycidyltrimethylammonium chloride (GTC), lanthanum (III) nitrate hexahydrate, isopropanol solution and potassium phosphate monobasic were purchased from Sigma-Aldrich and used without further purification.

### 2.2. Adsorbent preparation for phosphate removal

#### 2.2.1. Preparation of the chitosan-wheat straw biochar composite

1) Preparation of wheat straw biochar

Wheat straw was collected from a farm in Yunnan province of southwest China. The straw was dried in an oven at 80 °C and then cut into pieces of 5 cm long. The pyrolization was performed in a tube furnace infused with $N_2$ flow, with increasing temperature at the gradient of 10 °C $min^{-1}$. The temperature was maintained at 550 °C for 30 min, before cooling under continuous $N_2$ flow. The produced biochar was grounded through a 150 μm mesh. Ash was removed by adding an aliquot of 10 g of the obtained biochar to 1L of 1 M HCl solution, stirred overnight, and finally washed 6 times with 2L of water for 30 min and dried at 60 °C in a vacuum oven.

2) Preparation of the composite of chitosan and wheat straw biochar

1 g of chitosan was added in 400 ml of 2% acetic acid solution and stirred 3 h at 40 °C and 450 rpm. 1 g of the prepared biochar was added to the solution and stirred 1 h at 40 °C and 450 rpm. The pH of the mixture was adjusted to 12 using 1 M NaOH and 0.1 M HCl, and further stirred for 2 h at 40 °C and 200 rpm. Finally, the mixture was filtered and washed with 4L of water, and dried at 60 °C in a vacuum oven. The obtained sample was designated as CB.

3) Direct cross-linking of CB with glutaraldehyde

1 g CB was added separately with glutaraldehyde at different glutaraldehyde/CB ratios of 0 ml $g^{-1}$, 0.1 ml $g^{-1}$, 0.25 ml $g^{-1}$, 0.5 ml $g^{-1}$ and 2.5 ml $g^{-1}$, respectively. The mixtures were stirred 5 h at 40 °C, and then filtered and washed with 4L of water. The prepared samples were denoted as $G_0$CB, $G_{0.1}$CB, $G_{0.25}$CB, $G_{0.5}$CB, $G_{2.5}$CB, respectively.

4) New cross-linking of CB with amine group protection

The new cross-linking process is as follow [8]:

a) Protection of the amine group on chitosan with formaldehyde.

1 g CB was added to 100 ml water and 100 ml of 37.8% formaldehyde solution. The mixture was subsequently stirred for 4 h, filtered, and washed with 4L of water. The obtained sample was denoted as FCB.

b) Cross-linking of FCB with glutaraldehyde.

1 g FCB as prepared above was transferred to 200 ml water solution, and the pH was adjusted to 12 with 0.1 M NaOH solution and 0.1 M HCl. Following, a certain amount of glutaraldehyde solution was added. Herein, the amount of glutaraldehyde was 0.5, 1.5, 2.5 ml, respectively. The mixtures were stirred 5 h at 40 °C, filtered, and washed with 4L of water. The cross-linked samples are short-named as $G_{0.5}$FCB, $G_{1.5}$FCB and $G_{2.5}$FCB, respectively.

c) Release of the protected amine group on GFCB.

The filtered GFCB samples were added to 200 ml of 0.5 M HCl solution in a 400 ml beaker, and stirred overnight. The mixture was filtered and washed with water, and added to 200 ml of 0.5 M NaOH solution let to stir for 6 h before washing with 4L of water. The obtained samples are denoted as $G_{0.5}FCB_{HCl}$, $G_{1.5}FCB_{HCl}$ and $G_{2.5}FCB_{HCl}$, respectively.

*2.2.2. Load of quaternary ammonium on $GFCB_{HCl}$*

2 g of $G_{2.5}FCB_{HCl}$ was added into 40 ml water and sonicated for 3 min. Following, the mixture was heated to 60 °C, and added drop by drop with 5 ml of GTC before additional stirring for 30 min. The slow addition of GTC was repeated until the total volume of GTC added reached 20 ml. Finally, the mixture was stirred 24 h at 60 °C, washed with 2L water through filter paper to remove the excess GTC and dried at 60 °C in a vacuum oven. The obtained sample is short-named as GTB.

*2.2.3. Load of La on GTB*

0.4 g of the oven-dried GTB was added to 15 ml of water and stirred 1 h at 60 °C. Meanwhile, 1 g $La(NO_3)_3{\cdot}6H_2O$ was added to 15 ml of isopropanol solution and stirred for 1 h at room temperature. The prepared La solution was slowly dropped into the GTB solution and left to react for 24 h at 60 °C, before adjusting the pH to 9 with 0.1 M NaOH and 0.1 M HCl. The mixture was stirred for 2 more hours at 60 °C, and for 48 more hours at room temperature, followed by filtering, 2L water-washing, and drying in a vacuum oven at 60 °C [19]. The obtained sample was named as La/GTB.

*2.3. Characterization of the prepared samples*

The prepared samples CB, FCB, $G_{2.5}$FCB, $G_{2.5}FCB_{HCl}$, and $G_{2.5}$CB were analyzed by Fourier Transform infrared spectroscopy (FTIR) (Thermo Scientific, NICOLET iS50) to determine the functional groups present on the surface. The samples were also analyzed by X-ray photoelectron spectroscopy (XPS, Kratos Axis Ultra DLD system).

*2.4. Phosphate adsorption experiment*

Adsorption experiments were carried out at various pH, equilibrium time, temperature, and initial phosphate concentration.

1) Adsorption at different pH.

A batch of 25 mg adsorbent was individually added into 50 ml of 100 mg P $L^{-1}$ phosphate solution at pH 2.5, 3, 4, 5, 6, and 7. The mixtures were shaken 24 h at 150 rpm.

2) Adsorption at different equilibrium time.

A batch of 25 mg adsorbent was added into 100 ml of 25 mg P $L^{-1}$, and 50 ml of 100 mg P $L^{-1}$ phosphate solutions at pH 3, in order to study the adsorption equilibrium time when adsorbent has the maximum adsorption capacity. Samples were shaken for different periods of time: 5 min, 10 min, 30 min, 60 min, 120 min, 240 min and 360 min.

3) Isothermal adsorption.

25 mg adsorbent was added into 50 ml phosphate solution. Experiments were performed varying initial phosphate concentration: 25, 50, 100, 200, and 300 mg P $L^{-1}$, respectively. Each test was performed at three temperatures: 15, 30, and 45 °C. The adsorptions were performed for 24 h, with the assistance of shaking.

4) Desorption studies.

Previous studies indicated that adsorbent materials modified with amine group or lanthanum have good regenerative capacity when a NaOH solution is utilized. Accordingly, we performed the desorption study utilizing a 0.1 M NaOH solution. Specifically, 500 mg La/GTB was added into 2 L of 25 mg P $L^{-1}$ phosphate solution. The mixtures were shaken at 150 rpm and after 24 h the samples were filtered and washed, prior to be transferred into 2 L of the 0.1 M NaOH solution. Samples were then shaken for another 48 h and filtered with water until reaching neutral pH. The obtained samples were vacuum dried at 60 °C before use. The above process was repeated three times.

After the experiment, phosphate concentration of the solution was measured by UV–Vis spectroscopy (Evolution 260 Bio UV–Vis spectrophotometer, Thermo Scientific) at the wavelength of 710 nm. The amount of phosphate adsorbed on the absorbent was calculated by the following equation:

$$q_e = \frac{V(C_0 - C_e)}{m} \quad (1)$$

where $q_e$ is the amount of phosphate adsorbed on the composite (mg $g^{-1}$); $C_0$ and $C_e$ are the initial and equilibrium concentration, respectively, of phosphate in the solution (mg $L^{-1}$); V is the volume of the solution (ml), and m is the amount of the adsorbent (g).

The calculation formula of the partition coefficient PC is as follows:

$$PC = \frac{Adsorption\ \ capacity}{Equilibrium\ \ Concentration} \quad (2)$$

where the adsorption capacity refers to the adsorption capacity of absorbent at equilibrium, mg $g^{-1}$, and the equilibrium concentration is the concentration of P in the solution at equilibrium, μ $M^{-1}$

## 3. Results and discussion

*3.1. Results of FTIR analysis*

Fig. 1 shows the FTIR spectra obtained (for an enlarged figure we refer the reader to Fig. S1, Supplementary material). 8 major bands

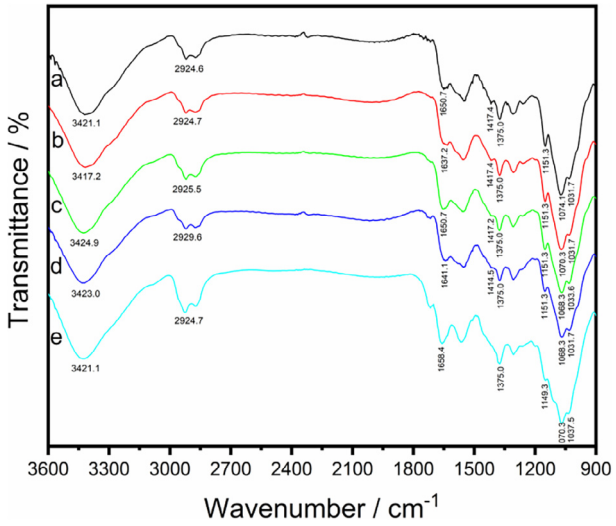


**Fig. 1.** FTIR spectra of CB (a), FCB (b), $G_{2.5}$FCB (c), $G_{2.5}FCB_{HCl}$ (d), $G_{2.5}$CB (e).

**Scheme 1.** Reaction of chitosan with formaldehyde for the amine group protection.

were identified for the spectrum of CB (Fig. 1, a). The strong and broad band around 3421.1 $cm^{-1}$ is the result of stretching vibration of the functional groups –NH and –OH. The band around 2924.7 $cm^{-1}$ is characteristic of aliphatic group of –CH and $–CH_2$ [8,20,21]. 1650.7 $cm^{-1}$ is the bending vibration of –NH in $–NH_2$, and 1417.4 $cm^{-1}$ is the deformation vibration of –NH in $–NH_2$ [8]. The band at 1375.0 $cm^{-1}$ indicates the symmetric blending vibration of –CH in –CHOH–. Finally, the band at 1151.3 $cm^{-1}$ indicates the stretching vibration of –CN, while the bands at 1074.1 $cm^{-1}$ and 1031.7 $cm^{-1}$ indicate the stretching skeletal vibration of C–O [8,22].

Protection of the amine group on the chitosan surface for CB using formaldehyde induced two kinds of change to the spectra (Fig. 1, b): first, a shifting of wavenumber and/or a weakening of the transmittance of the major bands. Specifically, the band around 3421.1 $cm^{-1}$, was shifted to 3417.2 $cm^{-1}$, while the peak at 1650.7 $cm^{-1}$ was shifted to 1637.2 $cm^{-1}$. The latter, as well as the peaks at 1417.4 $cm^{-1}$ and 1151.3 $cm^{-1}$, were also weakened. These changes were all related to the chemical bonds with nitrogen obtained as a result of the reaction of amine group with formaldehyde [8], which is represented in Scheme 1.

Cross-linking with glutaraldehyde after formaldehyde treatment weakened the peaks at 1417.2 $cm^{-1}$ and 1151.3 $cm^{-1}$ in comparison with the spectra of FCB (Fig. 1, c), suggesting that glutaraldehyde consumed some amine groups. The peak at 1637.2 $cm^{-1}$ was shifted to 1650.7 $cm^{-1}$, while strengthened slightly as a result of C = N stretching [23], which were obtained during the cross-linking process by Schiff's base reaction (Scheme 2b), due to reaction between the aldehyde ends of the cross-linker and the amine moieties [23,24], as represented in Scheme 2.

The FTIR spectrum obtained for the direct cross-linking of CB with glutaraldehyde without previous protection of amine groups is shown in Fig. 1e. The peak of $G_{2.5}$CB at 1658.4 $cm^{-1}$ was more strength and breadth than the peak of $G_{2.5}$FCB at 1650.7 $cm^{-1}$ (Fig. 1, c). This result suggests that a consistently higher number of amine groups reacted with the cross-linker to form the –C = N bond in comparison to the new cross-linking process. Meanwhile, the peaks of $G_{2.5}$CB at 1414.5 $cm^{-1}$ and 1151.3 $cm^{-1}$ were weakened significantly, due to the consumed amine group on the surface of chitosan. These results provide evidence that the amount of consumed amine group in the direct cross-linking method is higher than the consumed amine groups with the new cross-linking method described. This should be the reason why the adsorption capacity of the adsorbent crosslinked by the latter cross-linked method is slightly higher than the former.

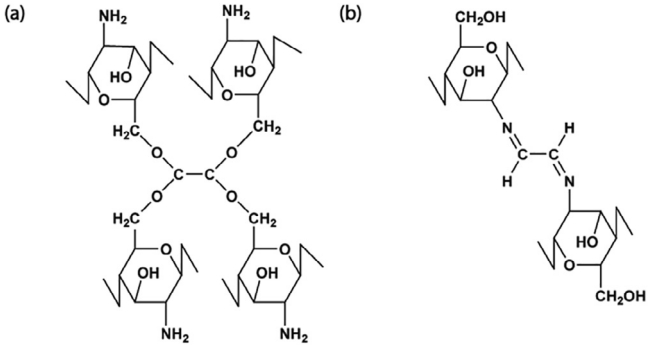

**Scheme 2.** Mechanism of the cross-linking process between chitosan and glutaraldehyde. (a) The aldehyde ends of glutaraldehyde after reaction with hydroxyl groups; (b) the aldehyde ends of glutaraldehyde after reaction with amine groups.

While some studies reported a peak at 1110 $cm^{-1}$ as a result of the reactions of the cross-linkers, glutaraldehyde, and glyoxal, with the hydroxyls on chitosan as a process of acetalization (Scheme 2a) [23,25]. This peak was not found in our analysis. suggesting that the hydroxyls on chitosan were perhaps not involved in the cross-linking reactions during our experiments. After removal of formaldehyde by treatment with HCl, the peak at 1650.7 $cm^{-1}$ in $G_{2.5}$FCB was shifted to 1641.1 $cm^{-1}$ (Fig. 1, d), suggesting that the protected amine group, $–N = CH_2$, was converted back to $NH_2$.

### 3.2. XPS analysis

Fig. 2 shows the obtained XPS 1 s spectra of O. Two peaks were revealed in the O 1 s XPS spectra of CB, one at 532.8 eV and one at 533.2 eV (Fig. 2, a), representing the oxygen-containing functional group –OH and C-O-C, respectively [26]. After formaldehyde treatment, the O 1 s peaks of FCB are similar to CB (Fig. 2, b), suggesting that the two functional groups on CB did not react with formaldehyde. The subsequent cross-linking with glutaraldehyde, however, shifted the peaks of 532.6 eV and 533.0 eV on FCB to 529.8 eV and 530.5 eV, respectively, and a new peak at 532.1 eV was obtained (Fig. 2, c). The new peak reflects the group C-O-C that may be produced in the reaction of glutaraldehyde with $–CH_2OH$ on chitosan (scheme 2, a) [8]. A similar peak was observed at 532.7 eV with $G_{2.5}$CB (Fig. 2, e), indicating that the same reaction also occurred in the direct cross-linking. In the latter case, however, the peak is much weaker than that for $G_{2.5}$FCB, indicating that the link with the group –OH is relatively weak in the direct cross-linking.

In the new cross-linking most of the amine groups are unavailable for glutaraldehyde, due to the protection and thus, more –OH group acted as the substitute, giving rise to a stronger peak at 532.1 eV. After release of the amine group by HCl, the resulted $G_{2.5}FCB_{HCl}$ shows no significant change with the peak of 532.1 eV (Fig. 2, d), suggesting that the HCl treatment has no significant effect on the linking between glutaraldehyde and $–CH_2OH$ (C-O-C, 532.1 eV). Nevertheless, treatment of $G_{2.5}$FCB with HCl strengthened the peak at 530.5 eV (Fig. 2, c), suggesting that the reaction increased oxygen-related groups such as C-O-C, probably due to oxidation to $G_{2.5}$FCB. The N 1 s XPS spectra are shown in Fig. 3. CB showed a single peak at 400.3 eV (Fig. 3, a), due to the functional group $–NH_2$ [22]. After formaldehyde treatment, 2 peaks were observed at 399.5 eV and 401.2 eV (Fig. 3, b). The former reflected the group $–N = CH_2$ and the latter $–NH_2$ [8]. Formation of the functional group $–N = CH_2$ resulted from the reaction of $–NH_2$ on chitosan with formaldehyde following Scheme 1, further confirming amine group protection on chitosan. Cross-linking with glutaraldehyde shifted the peak from 399.5 eV to 397.1 eV, but did not affect peak intensity (Fig. 3, c), proving that the amine groups were not cross-linked after the protection. Meanwhile, two new peaks were observed at 398.3 eV and 399.0 eV, belonging to amide (–NH) and protonated amine ($–N^+$), respectively [27], produced during the cross-linking. The subsequent treatment of $G_{2.5}$FCB with HCl moved the peak 397.1 eV ($–N = CH_2$ groups) to 396.8 eV (Fig. 3, d). The bonding energy of 396.8 eV is the same as the $G_{2.5}$CB ($–NH_2$) (Fig. 3, e), confirming that the $–N = CH_2$ group on $G_{2.5}$FCB were converted back to $–NH_2$. Meanwhile, a small peak occurred at 397.2 eV (Fig. 3, d), associated with the group $–N = CH_2$, indicating that a small portion of the protected amine group was not recovered after the acid treatment.

The XPS analysis of La/GTB proved the successful loading of La on GTB by the two representative satellite peaks of La $3d_{5/2}$ at 835.2 eV and 831.9 eV (Fig. 4, left). The doublet satellite peaks are commonly observed at high energy in La-based hydr (oxides) possibly due to charge transfer from the valence band of the ligand atom to the 4f orbital of the La atom [28].

The standard XPS P 2p spectrum peaks are obtained at 134.eV for

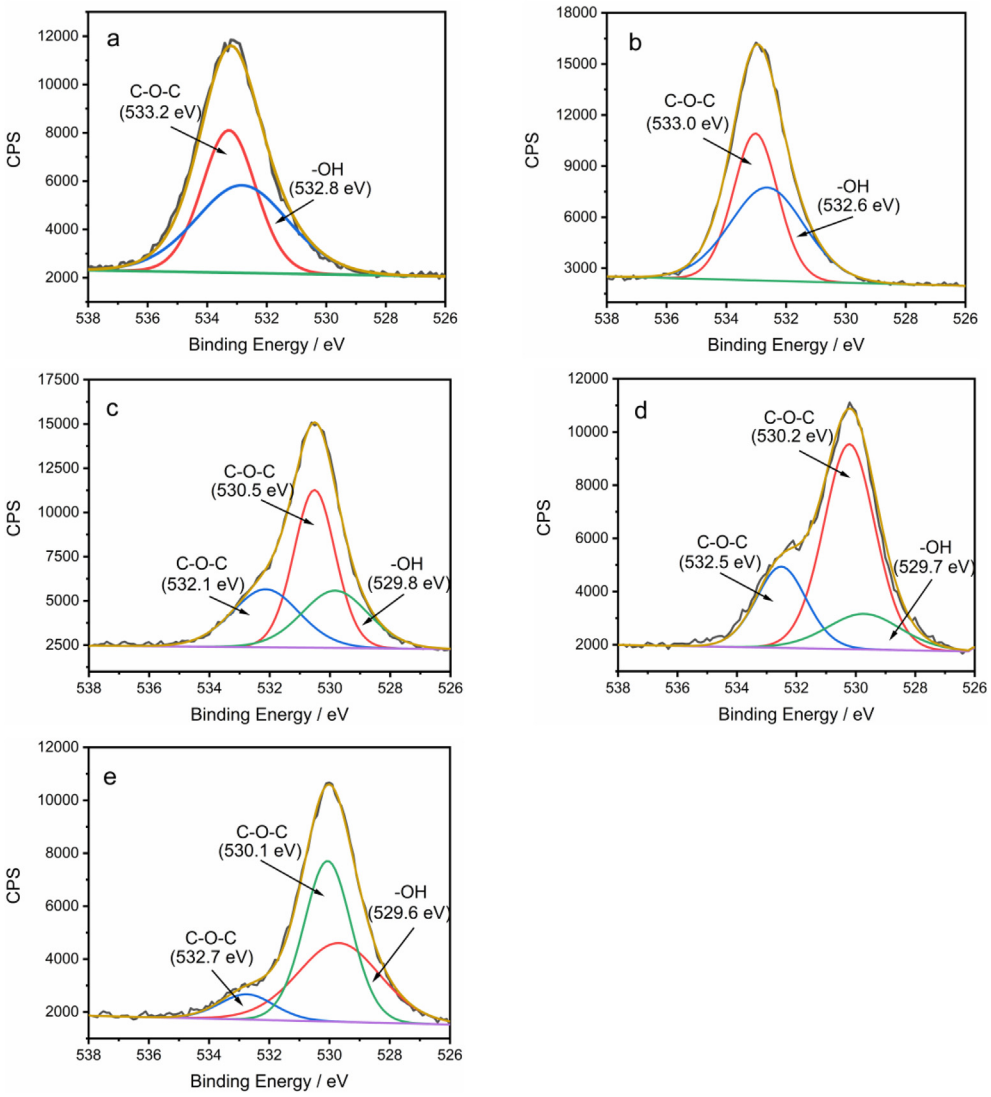


**Fig. 2.** XPS 1 s spectra of O for CB (a), FCB (b), $G_{2.5}FCB$ (c), $G_{2.5}FCB_{HCl}$ (d) and $G_{2.5}CB$ (e).

phosphate in pure $KH_2PO_4$ [29]. After adsorbed on La/GTB, the P 2p peak was observed at ~129.7 (Fig. 3, b). The shift towards low energy by 4.3 eV results from the strong affinities between phosphate and the adsorbent [29]. Two more peaks were observed at 130.4 eV and 129.5 eV, both representing the phosphate-La/GTB complex. The former stands for the species of $LaPO_4$, while the latter for the phosphate-loaded quaternary ammonium group [28].

### 3.3. Optimal quantity of the cross-linking agent

#### 3.3.1. Direct cross-linking

Glutaraldehyde is a frequently used cross-linker; however, the quantity used to cross-link chitosan is critical. As shown in Fig. 5, the adsorption capability of GCB increased from $G_0CB$ through $G_{0.1}CB$ to $G_{0\cdot25}CB$, and then decreased from $G_{0\cdot25}CB$ through $G_{0.5}CB$ to $G_{2.5}CB$ at pH 3. As expected, the minimum capability occurred when cross-linking was not performed, due to the solubility of chitosan in the acidic solution. Strengthening the cross-linking increased the adsorption capability. After reaching maximum capability at 0.25 ml of glutaraldehyde, the cross-linker reacted with the functional group $NH_2$, reducing the adsorption performance despite the improvement on the adsorbent's stability [10]. These results clearly indicate the optimal cross-linking in our experiments.

Solution pH affects the adsorption process as a result of its dominance over the equilibrium between different species of phosphate, and thus, it is important for the evaluation of the optimal cross-linking. The maximum adsorption capability occurs at pH 3 (Fig. 6), because the species are predominantly in the form of $H_2PO_4^-$, which is easily adsorbed by chitosan compared to other species [30]. As the pH of solution exceeds 4, which is higher than the pH threshold of chitosan dissolution [7], the adsorption capability of $G_0CB$ or slightly cross-linked composites (such as $G_{0.1}CB$) should significantly increase since the amino groups in the chitosan surface are in the free from, or minimally bonded with the cross-linker. Therefore, the adsorption of $G_0CB$ should be higher than those cross-linked at pH over 4. The results, however, show that the best adsorbent is $G_{0.1}CB$ at pH 5, and $G_{0.25}CB$ for pH ≥ 6, confirming that proper cross-linking improves the adsorption performance of chitosan.

#### 3.3.2. New cross-linking process

As shown in Fig. 7, the maximum phosphate adsorption of $G_{0.5}FCB_{HCl}$, $G_{1.5}FCB_{HCl}$ and $G_{2.5}FCB_{HCl}$ was 39.9 ± 0.9 mg P $g^{-1}$, 43.4 ± 2.2 mg P $g^{-1}$, and 43.7 ± 0.4 mg P $g^{-1}$, respectively, making the adsorption by $G_{0.5}FCB_{HCl}$ the lowest among the three. The main reason lies in its poor stability in the acidic solution, and partial dissolution was observed, thus preventing further experiments with lower amounts of glutaraldehyde. Since glutaraldehyde only affects the unprotected amine groups on chitosan during cross-linking, these results

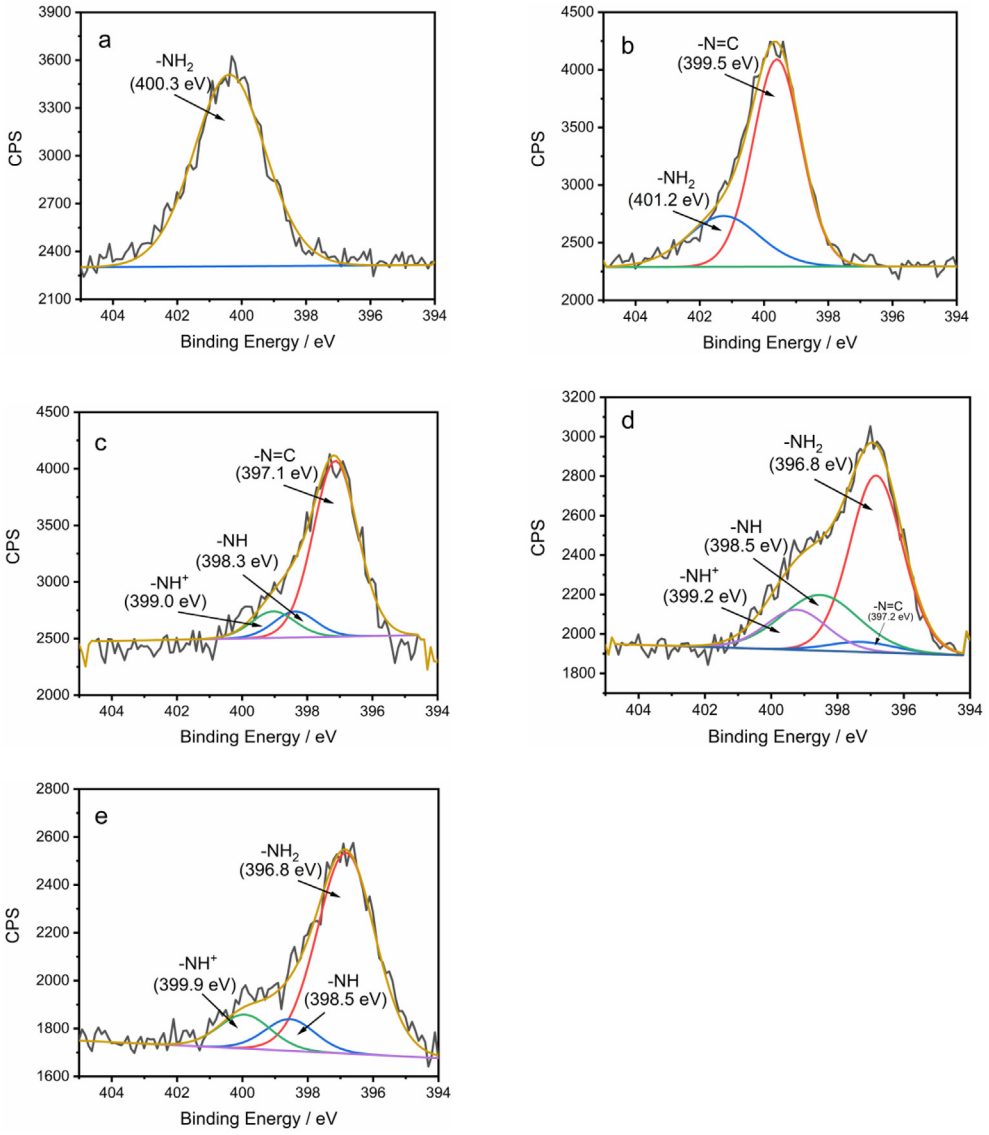


**Fig. 3.** XPS 1 s spectra of N for CB (a), FCB (b), $G_{2.5}$FCB (c), $G_{2.5}FCB_{HCl}$ (d) and $G_{2.5}$CB (e).

suggest that 0.5 ml glutaraldehyde was not sufficient to react with the unprotected $NH_2$ group. Conversely, the adsorption capacities of $G_{1.5}FCB_{HCl}$ and $G_{2.5}FCB_{HCl}$ were similar. The quantity of unprotected amine groups should be the same for $G_{1.5}FCB_{HCl}$ and $G_{2.5}FCB_{HCl}$, since the same protection procedure was performed. Accordingly, the similar adsorption capacity suggests that 1.5 ml of glutaraldehyde is sufficient to consume all the unprotected amine groups, and further increase of glutaraldehyde has no influence on the adsorption. As a result, the effective amine groups are the same after recovery with HCl.

### 3.3.3. Comparison of direct and new cross-linking processes

The discussion of the advantages of new cross-linking methods over the direct cross-linking was often done through a comparison for adsorption capacity on the same amount of the cross-linker. Li et al. [8] investigated the direct cross-linking and the new cross-linking methods with the same amount of cross-linking agents, suggesting that the adsorption capability of the adsorbent could be significantly increased by the new cross linking. The above results on the optimal quantity of the cross-linker, however, suggested that this evaluation can be misleading since the optimal adsorption occurred at different amount of glutaraldehyde in the two cross-linking processes. Taking 2.5 ml of glutaraldehyde as an example, the adsorption capacity of $G_{2.5}FCB_{HCl}$ is systematically higher than that of $G_{2.5}$CB. The increasing adsorption rate is 225% on average, and as high as 663% at pH 7 (Fig. 8), clearly indicating the advantages of the new cross-linking process. However, it should be considered that the optimal adsorption capacity by the direct cross-linking took place at a much lower amount of glutaraldehyde, specifically 0.25 ml. Going from 0.25 ml to 2.5 ml, the capacity of GCB was decreased by 38% at pH 3. Therefore, the choice of two cross-linking methods depends on the purpose of using chitosan. Specifically, the new crosslinking methods are of particular interest when a limited number of amino groups in the adsorbent material is the determining factor. On the contrary, when the minor loss of amine groups is not taken into account, the direct crosslinking could be applied.

### 3.4. Adsorption by $G_{2.5}FCB_{HCl}$, GTB and La/GTB

Phosphate adsorptions for $G_{2.5}FCB_{HCl}$, GTB, and La/GTB at different initial pH are reported in Fig. 9. $G_{2.5}FCB_{HCl}$ showed the highest phosphate adsorption at pH 3, with a maximum capacity of 43.7 ± 0.4 mg P $g^{-1}$. The adsorption decreased rapidly with pH, reaching 5.9 ± 1.4 mg P $g^{-1}$ at pH 7. Once modified with the quaternary ammonium, the adsorption of the composite was significantly improved, especially its effective range of pH, which was extended pH 7. The

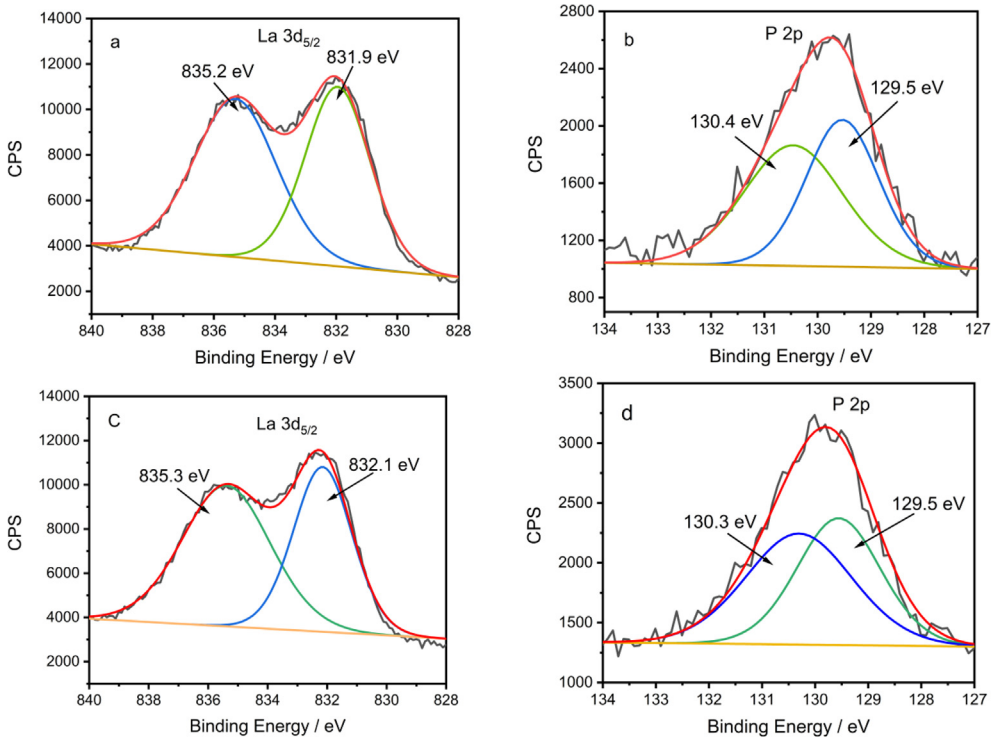


**Fig. 4.** XPS La $3d_{5/2}$ spectra of La/GTB (a) and XPS P 2p spectra of La/GTB after phosphate adsorption (b). XPS La $3d_{5/2}$ spectra of La/GTB (c) and XPS P 2p spectra of La/GTB after desorption (d).

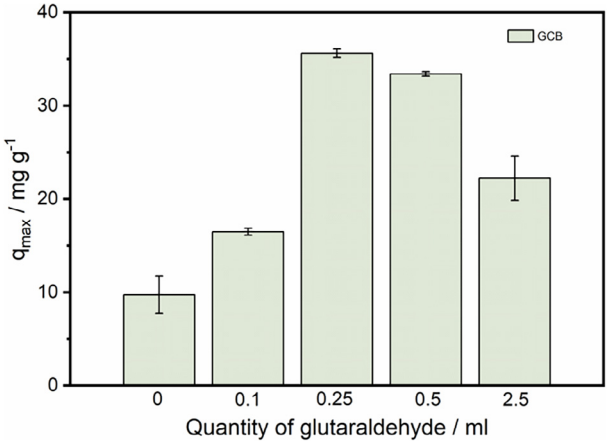


**Fig. 5.** Adsorption capabilities of GCB with increasing amounts of glutaraldehyde in the direct cross-linking process.

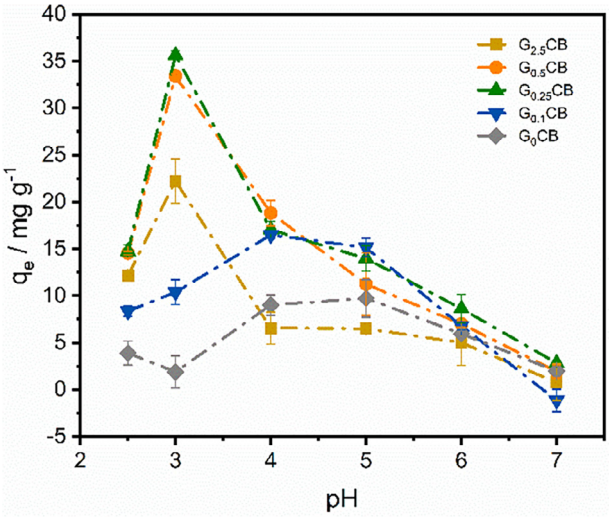


**Fig. 6.** pH effect on the adsorption capability of GCBs that were directly cross-linked.

optimal capacity occurred at pH 5 (40.4 ± 0.4 mg P $g^{-1}$), but the result to be underlined is the adsorption at pH 7, which was as high as 26.4 ± 0.9 mg P $g^{-1}$, over 4 times higher than $G_{2.5}FCB_{HCl}$ for the same pH. Clearly, modification with quaternary ammonium widened the effective pH of the composite, and raised the adsorption capacity from pH 4 to pH 7.

These characteristics were even strengthened by further modification with Lanthanum hydroxide. In fact, the optimal adsorption capacity of La/GTB was 86.7 ± 1.6 mg P $g^{-1}$, more than double of the capacity of GTB. Furthermore, the effective pH was shown to be extended from pH 2.5 to pH 7, and compared to GTB, little changes occurred to the adsorption capability in the whole range of pH.

### 3.5. Adsorption kinetics

The time needed to reach adsorption equilibrium is an important factor for the evaluation of an adsorbent's performance. As shown in Fig. 10, the adsorption of La/GTB increased rapidly in the incipient stage of contact. At 100 mg P $L^{-1}$, which represented high initial P concentration, the equilibrium time was 30 min, and 96% of the adsorption was achieved in the first 5 min. At 25 mg P $L^{-1}$, exemplifying low P concentrations, 75% of the total adsorption was reached in 5 min, increasing to 93% in 30 min despite that the equilibrium was attained in 2 h. Accordingly, the equilibrium time was shortened significantly by the procedures reported in this work compared to the reported equilibrium times involving phosphate adsorption by lanthanum hydroxide modification in literature (Table S3, i.e. 60 min in 100 mg P $L^{-1}$ [31], 6 h in 30 mg P $L^{-1}$ [32] and 12 h in 20 mg P $L^{-1}$ [19]).

Another important aspect to consider when assessing the

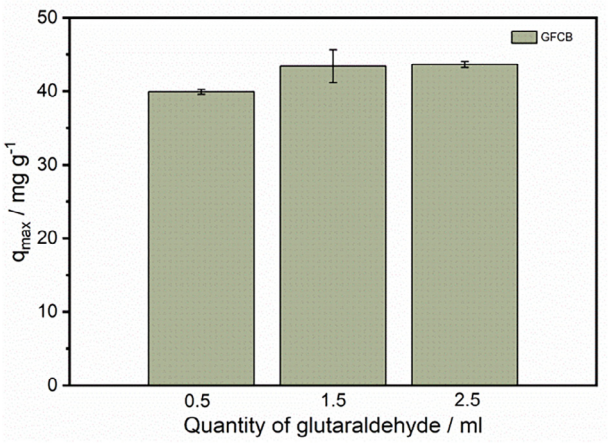


**Fig. 7.** The maximum phosphate adsorption of $G_{0.5}FCB_{HCl}$, $G_{1.5}FCB_{HCl}$ and $G_{2.5}FCB_{HCl}$ at pH 3.

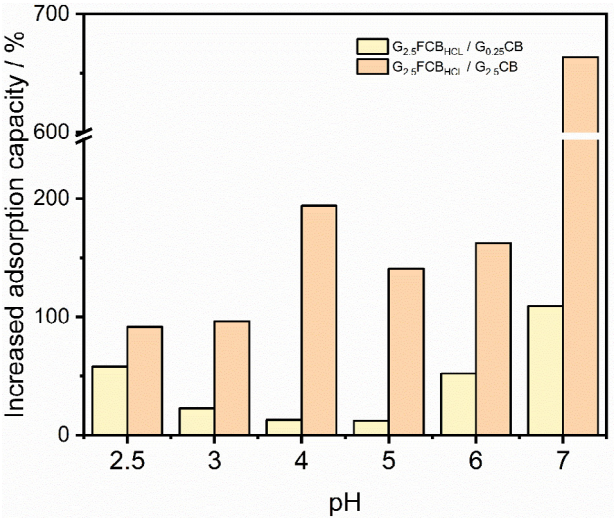


**Fig. 8.** Increase of phosphate adsorption obtained with the new cross-linking process relative to the direct cross-linking for different amounts of cross linker. (Initial P: 100.0 mg $L^{-1}$; Adsorption dose: 0.25 g $L^{-1}$; Temperature: 30 °C; T = 24 h).

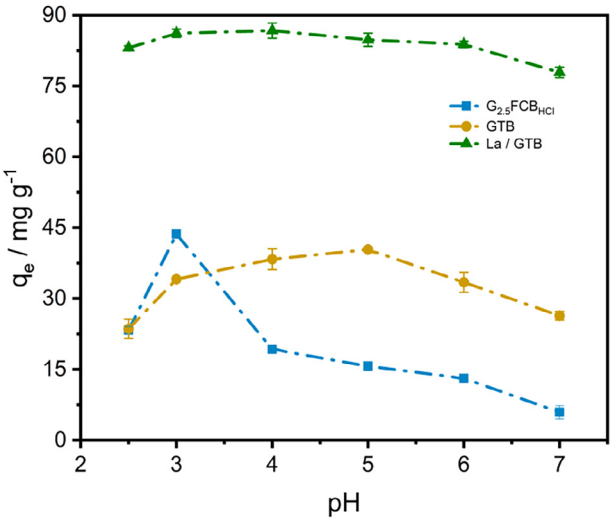


**Fig. 9.** Adsorption of phosphate by $G_{2.5}FCB_{HCl}$, GTB and La/GTB at different initial pH of the solution (Initial P: 100.0 mg $L^{-1}$; Adsorption dose: 0.25 g $L^{-1}$; Temperature: 30 °C; T = 24 h).

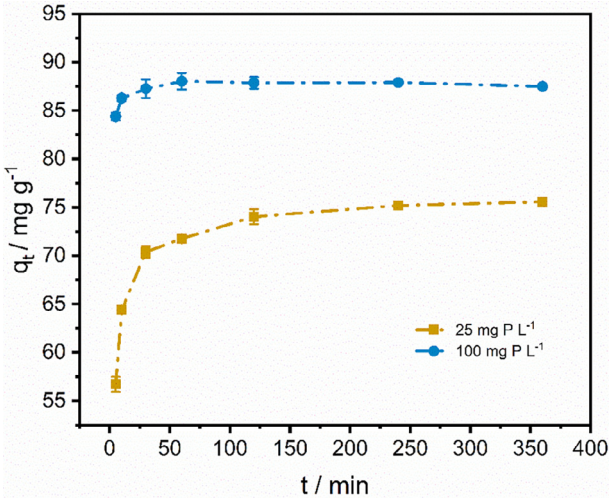


**Fig. 10.** Kinetics of phosphate adsorption by La/GTB. (Initial P: 25 and 100 mg $L^{-1}$; Adsorption dose: 0.25 g $L^{-1}$; Temperature: 30 °C; pH: 3; T = 5 min, 10 min, 30 min, 60 min, 120 min, 240 min, 360 min).

performance of an adsorbent is the adsorption rate. To better define the performance of La/GTB in this regard, the kinetic data were fitted into pseudo-first-order and pseudo-second -order models [7]:

$$q_t = q_e(1 - exp(-k_1 t)) \quad (3)$$

$$\frac{t}{q_t} = \frac{1}{K_2 q_e^2} + \frac{t}{q_e} \quad (4)$$

Where t is time (min), $q_t$ (mg $g^{-1}$) and $q_e$ (mg $g^{-1}$) are adsorption capacity of adsorbent at time t and at equilibrium, respectively. $k_1$ ($min^{-1}$) and $k_2$ (g $mg^{-1}$ $min^{-1}$) are rate constants, respectively.

The valve of kinetic parameters was listed in Table S1. The fitting results indicated that the pseudo-second-order model better described the experimental data ($R^2 > 0.99$) compared to the first-order ($R^2 > 0.82$), suggesting that the adsorption is a chemisorption process.

### 3.6. Adsorption isotherms

The results of adsorption isotherms showed that the adsorption capability of La/GTB increased from 51.5 ± 0.2 mg $g^{-1}$ to 92.2 ± 1.2 mg $g^{-1}$ in the series of initial concentration at 15 °C (Fig. 11). Similar increase with the concentration was also found at 30 and 45 °C. When analyzing a specific concentration, however, temperature makes no significant difference to the adsorption process ($P > 0.05$), suggesting that they do not affect the performance of La/GTB. Therefore, when used for on-site phosphate pollution treatment, application of La/GTB can be carried out irrespective of water temperatures.

Despite that the adsorption capacity increases with the concentration of P in solution, the removal rate of the pollutant decreased following a natural logarithmic function (Fig. 12). It should be noted that at 25 mg P $L^{-1}$, a 100% phosphate removal can be obtained, indicating that La/GTB works well in low concentration.

Langmuir and Freundlich isotherms [31] were both used to fit the adsorption isotherm data (Table S2).

$$\frac{C_e}{q_e} = \frac{1}{K_L q_m} + \frac{1}{q_m} C_e \quad (5)$$

$$\log\ q_e = \log\ K_F + \frac{1}{n} \log\ C_e \quad (6)$$

where $q_m$ and $q_e$ are maximum adsorption capacity (mg $g^{-1}$) and the corresponding adsorption capacity (mg $g^{-1}$), respectively. *Ce* is the equilibrium phosphate concentration in solution (mg P $L^{-1}$). $K_L$ and $K_F$

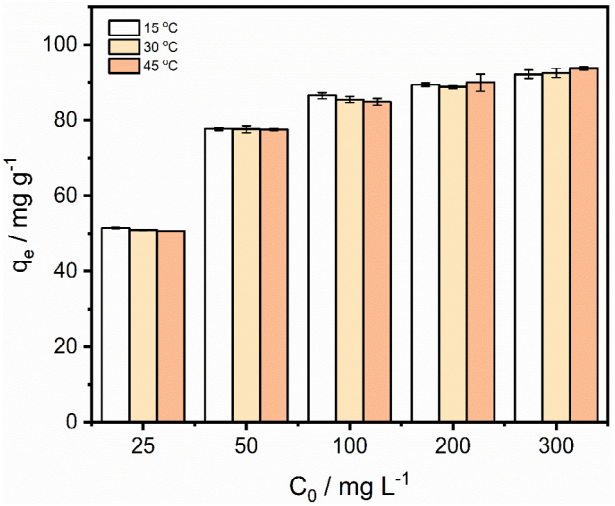


**Fig. 11.** Phosphate adsorption isotherms of La/GTB. (Initial P: 25, 50, 100, 200, 300 mg $L^{-1}$; Adsorption dose: 0.25 g $L^{-1}$; Temperature: 15, 30, 45 °C; pH: 5; T = 24 h).

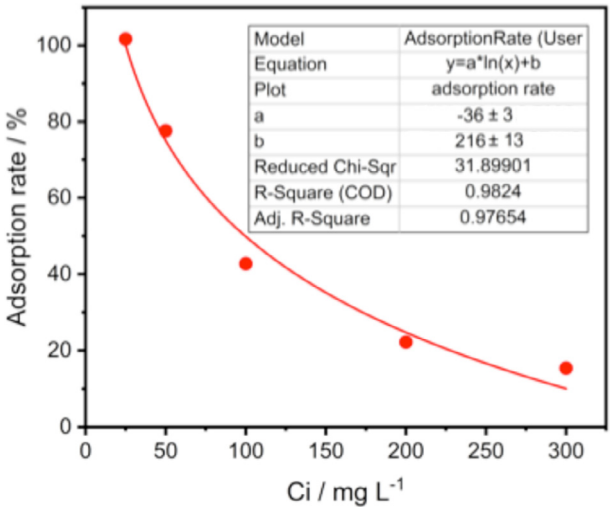


**Fig. 12.** Change of the adsorption rate of La/GTB with phosphate concentration in the solution.

are Langmuir constants and Freundlich constants, respectively.

The Langmuir model fits the data better ($R^2$ > 0.998) than the Freundlich model ($R^2$ > 0.961), suggesting the phosphate adsorption is a monolayer process taking place on the surface of La/GTB. The best-fitted maximum adsorption was 108.86 ± 4.3 and 94.64 ± 0.42 mg P $g^{-1}$ at pH 3 and pH 5, respectively. Furthermore, the difference is not significant (P: 0.043 > 0.01), proving again that pH (in a range from 3 to 7) is not important in the adsorption of La/GTB as previously shown in Fig. 8.

### 3.7. Partition coefficient

It should be noted that the evaluation of the adsorption performance between different adsorbent materials focusing only on the adsorption capacity concept is limited [33]. Different experimental conditions during the adsorption can strongly affect the adsorption capacity, especially since the latter is very sensitive to the initial loading of pollutants and usually increases with increasing initial concentration. Therefore, comparing the adsorption capacities of adsorbents obtained from different experimental conditions could only provide little insights [34].

The partition coefficient (PC) for a solid-liquid adsorption system represents the ratio of the concentration of the adsorbate in the solid adsorbent phase to the concentration in the liquid phase at equilibrium, which can better indicate the performance of the adsorbent [35]. A comparison based on the PC is suitable for the adsorption evaluation under different experimental conditions, especially with different initial concentration levels [34].

Therefore, we evaluated the adsorption performance of La/GTB (Table 1) and compared it with the performance of other adsorbent materials reported (Table 2).

The partition coefficients of La/GTB at different concentrations are shown in the Table 1. The PC of La/GTB drops sharply with the increase of the initial concentration, as shown in Table 1. When the initial concentration is 25 mg $L^{-1}$, the PC value is 172.1 mg $g^{-1}$ $\mu M^{-1}$. However, an increase of the initial concentration to 300 mg $L^{-1}$ resulted in a PC of only 0.011 mg $g^{-1}$ $\mu M^{-1}$. The drastic difference in PC values is motivated by the fact that the adsorption site on the surface of the adsorbent is near saturation at high phosphorus concentration, and if the initial concentration is further increased, the adsorption capacity cannot remain unchanged, resulting in a significant drop in the PC value.

The partition coefficient can reduce the deviation in the performance evaluation of different adsorbents, by no longer considering only the maximum adsorption capacity, but more comprehensively considering the practical performance of the adsorbent. This approach contributes to study the feasibility of material application and determine if the adsorbent is suitable for the actual application in the environment [33]. As can be seen from Table 1, although the adsorption amount of La/GTB can be as high as 92.51 mg $g^{-1}$ at initial concentration 300 mg $L^{-1}$, the PC is only 0.011 mg $g^{-1}$ $\mu M^{-1}$, indicating that a large amount of phosphate remained in solution. However, at a low initial concentration of 25 mg $L^{-1}$, the adsorption capacity is 49.98 mg $g^{-1}$, and the PC value is as high as 172.1 mg $g^{-1}$ $\mu M^{-1}$, indicating that La/GTB has a great removal effect at low phosphorus concentrations. The above PC results show that La/GTB is more suitable for low-concentration phosphorus removal than high-concentration p-contamination, a condition that is relevant for phosphate pollution in the environment, indicating that the developed La/GTB is suitable for the treatment of water pollution.

Nehra et al. [34] summarized the PC values of some adsorbent materials for phosphorus adsorption, which we quote as a reference for evaluating the adsorption performance of La/GTB. In addition, we summarized and listed the ratio for adsorbent amount and solution

**Table 1**
Performance of La/GTB for phosphate removal.

| Adsorption condition °C, pH | The ratio mg $ml^{-1}$ | initial concentration μ $M^{-1}$ | Maximum removal efficiency % | Equilibrium concentration μ $M^{-1}$ | Maximum adsorption capacity mg $g^{-1}$ | PC mg $g^{-1}$ $\mu M^{-1}$ |
|---|---|---|---|---|---|---|
| 30, 5 | 0.5 | 806.45 | 99.98 | 0.29 | 49.98 | 172.1 |
| 30, 5 | 0.25 | 806.45 | 76.5 | 189.00 | 76.5 | 0.4048 |
| 30, 5 | 0.5 | 1612.90 | 77.6 | 361.03 | 77.61 | 0.2149 |
| 30, 5 | 0.5 | 3225.81 | 42.7 | 1847.61 | 85.45 | 0.0462 |
| 30, 5 | 0.5 | 6451.61 | 22.2 | 5018.52 | 88.85 | 0.0177 |
| 30, 5 | 0.5 | 9677.42 | 15.4 | 8185.26 | 92.51 | 0.0113 |

**Table 2**
Performance of other adsorbents for phosphate removal.

| Adsorbent | Adsorption condition | The ratio | initial concentration | Maximum removal efficiency | Equilib-rium concent-ration | Maximum adsorption capacity | PC | Ref. |
|---|---|---|---|---|---|---|---|---|
| | °C, pH | mg $ml^{-1}$ | μ $M^{-1}$ | % | μ $M^{-1}$ | mg $g^{-1}$ | mg $g^{-1}$ $\mu M^{-1}$ | |
| Iron-zirconium/activated carbon nanofiber | 25, 4 | – | 315.89 | 22.5 | 244.81 | 26.3 | 0.11 | [36] |
| Zirconium ions/chitosan beads | 15,4 | 0.2 | 210.59 | 61.27 | 81.56 | 61.7 | 0.76 | [37] |
| MIL-101(Fe) | 20, – | – | 6.32 | 92.5 | 0.47 | 227.22 | 227.22 | [38] |
| Dipolar grafted hydroxyethyl cellulose | 50, 5 | 0.25 | 1263.56 | 99.45 | 6.99 | 46.94 | 6.72 | [39] |
| Ferrihydrite-coated and lanthanum-decorated magnetite | 25, 6.28 | 1 | 1052.96 | 74.4 | 269.56 | 44.8 | 0.17 | [40] |
| MIL-100(Fe) | 25, 4 | 0.07 | 84.24 | 93.05 | 5.85 | 93.55 | 15.98 | [34] |

volume obtained for the related references in Table 2. As shown in Table 2, different absorbents reported were effective in the removal of phosphate, such as chitosan beads, activated carbon fiber, and metal materials. Compared to those studies, La/GTB exhibits excellent adsorption performance at lower phosphate concentration. Furthermore, when developing an adsorbent material for application in the field, other aspects must be taken into account. The wheat straw biochar modified in this study is more advantageous in terms of availability of the material source, price, and additional benefits such as high value recycling use of biomass wastes, making it a great candidate.

### 3.8. Desorption studies

Regeneration capacity is one of the most important factors to be considered in all adsorbents, since the recycling of adsorbents can reduce the cost, also enable recovery and utilization of adsorbate [7]. The adsorption-desorption experiment was carried out to explore the reusability of the adsorbent. However, the experimental results showed that the adsorbent only had 34% adsorption capacity in the second cycle compared with the first adsorption capacity. In order to study the reasons for the low regenerative capacity of the adsorbent, we did XPS analysis of La/GTB after desorption. The result was shown in Fig. 3. P 2p peak were still observed on the surface of La/GTB after desorption (Fig. 3, d), indicating that the binding between La and P is very stable, and most of the p adsorbed on the surface of La/GTB was not successfully resolved into the solution by 0.1 NaOH solution. A good aspect of the stable binding between La and P is that it is advantageous for phosphate adsorption of La/GTB in P -containing water pollution, but the negative counterpart is the complex recycling of La/GTB. Therefore, future research will be focused on developing efficient desorption methods.

### 3.9. Mechanism of La/GTB adsorption

As manifested in Fig. 13, the adsorption of anionic pollutant was performed in three ways: Electrostatic interaction, Ligand exchange and Lewis acid-base interaction.

#### 3.9.1. Electrostatic interaction

Physical electrostatic adsorption occurs when contact is given between the negatively charged phosphate and the positively charged

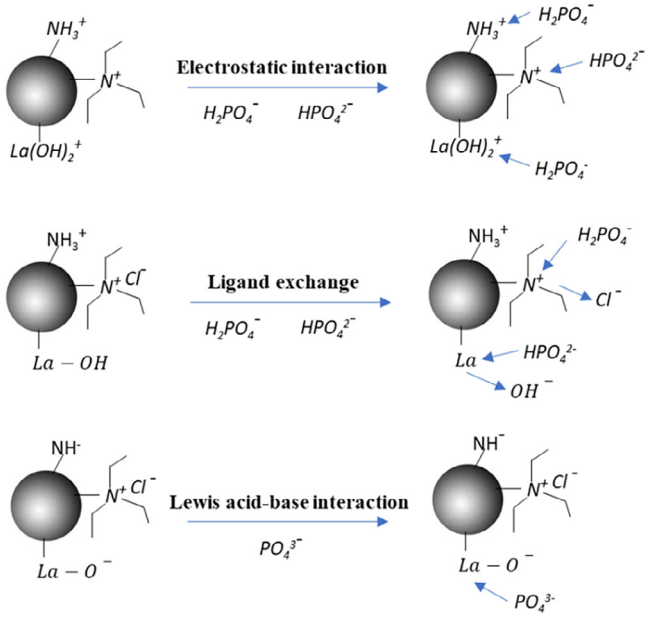


**Fig. 13.** Adsorption mechanism of La/GTB.

functional groups on the surface of the adsorbent [7]. At low pH value, the amine groups and quaternary ammonium groups on La/GTB are readily protonated [41]. Meanwhile, the hydroxyl groups can also become positively charged through the process: [32].

$$La - OH + H^+ \leftrightarrow La - OH_2^+ \quad (7)$$

The positively charged groups on the surface of La/GTB make electrostatic interaction a major mechanism for adsorption of the negatively charged P species such as $H_2PO_4^-$, $HPO_4^{2-}$ and $PO_4^{3-}$.

### 3.9.2. Ligand exchange

Ligand exchange happens between the negatively charged functional groups on the surface of the adsorbent and phosphate in solution [15]. Considering the functional groups on the surface of La/GTB, it is believed that ligand exchange should occur between the quaternary ammonium groups and phosphate, following the chemical equation:

$$R^+Cl^- + H_2PO_4^- \rightarrow R^+H_2PO_4^- + Cl^- \quad (8)$$

The hydroxyl group on the La binding site, which is more prone to be exchanged than those in the solution [4], provided another site for ligand exchange. The negatively charged phosphate species exchange with the hydroxyl groups of LaOH, releasing –OH to the solution following the reactions [42]:

$$La - OH + H_2PO_4^- \leftrightarrow La - H_2PO_4^- + OH^- \quad (9)$$

$$La = OH + HPO_4^{2-} \leftrightarrow La = HPO_4 + 2OH^- \quad (10)$$

$$La \equiv OH + PO_4^{3-} \leftrightarrow La \equiv PO_4 + 3OH^- \quad (11)$$

### 3.9.3. Lewis acid-base interaction

Lewis acid-base interaction occurs when the metal active site reacts with the oxygen anion of phosphate, forming metal-oxygen coordination [4]. The strong Lewis acidic property of La makes it attractive to the oxyanion of phosphate through this mechanism [15].

Lewis acid-base interaction may have played a critical role in phosphate adsorption at high pH values [15], at which the electrostatic interaction may not occur due to strong electrostatic repulsion. This can be explained considering that the amine groups, quaternary ammonium groups and La active sites on La/GTB are deprotonated and negatively charged at high pH. Meanwhile, ligand exchange was also weakened due to the deprotonation on the surface of the composite [32]. In these circumstances, the Lewis acid-base interaction may follow the reaction [15]:

$$biochar - -La^{n+} + PO_4^{3-} \rightarrow biochar - -LaOPO_3^{n-3} \quad (12)$$

## 4. Conclusions

We reported the successful wheat straw biochar modification with quaternary chitosan and lanthanum for enhanced phosphate removal in environmentally relevant conditions. The maximum phosphate adsorption capacity of the composite was 109 ± 4 mg P $g^{-1}$. A 100% adsorption equilibrium was reached for 100 mg P $L^{-1}$ and a 93% for 25 mg P $L^{-1}$ in 30 min, significantly shortening the time required for the process compare to other reports. Furthermore, the adsorption process was not impacted by temperature (15–45 °C) or pH (2.5–7). Even at pH 7, the composite maintained a high phosphate adsorption capacity, of 77.9 ± 1.1 mg P $g^{-1}$. These advantages are critical to achieve the application in the field of the presented composite. The partition coefficient was employed for evaluating the adsorption performance of La/GTB. The highest PC of La/GTB was 172.1 mg $g^{-1}$ $\mu M^{-1}$, which also proves that La/GTB is suitable for phosphorus pollution treatment in the real environment.

The adsorption capacity of different adsorbents was evaluated by direct cross-linking and a new cross-linking method, revealing that the optimum amount of crosslinker for the two approaches is different, an aspect that should be considered when comparing adsorption methods.

## Acknowledgments

The authors would also like to acknowledge the financial support from China under the name of the National Natural Science Foundation of China (U1612441) (X.L.), Sino-Israeli Intergovernmental Scientific and Technological Cooperation Project (2015DFG92450) (X.L.), Opening Fund of the State Key Laboratory of Environmental Geochemistry (SKLEG2016905) (S.D.M.), the 2014 Cooperative Project Between the Chinese Academy of Sciences and the Xinjiang Autonomous Region (X.L.) and the State Scholarship Fund from the China Scholarship Council (Y. H.). Thanks are also extended to the United States National Science Foundation, under award number 1561427 (F.C.M. and S.D.M.) for financial support.

## Associated content

Supporting information: The Supporting Information is available free of charge on the Elsevier Publications Website at XX. Kinetics of phosphate adsorption on La/GTB. Adsorption isotherms of La/GTB.

## Appendix A. Supplementary data

Supplementary data to this article can be found online at https://doi.org/10.1016/j.cej.2019.122375.

## References

[1] D.K. Veni, P. Kannan, T.N.J.I. Edison, A. Senthilkumar, Biochar from green waste for phosphate removal with subsequent disposal, Waste Manage. 68 (2017) 752–759.
[2] K. Vikrant, K.-H. Kim, Y.S. Ok, D.C.W. Tsang, Y.F. Tsang, B.S. Giri, R.S. Singh, Engineered/designer biochar for the removal of phosphate in water and wastewater, Sci. Total Environ. 616–617 (2018) 1242–1260.
[3] H. Liu, W. Guo, Z. Liu, X. Li, R. Wang, Effective adsorption of phosphate from aqueous solution by La-based metal–organic frameworks, RSC Adv. 6 (2016) 105282–105287.
[4] J. Liu, Q. Zhou, J. Chen, L. Zhang, N. Chang, Phosphate adsorption on hydroxyl–iron–lanthanum doped activated carbon fiber, Chem. Eng. J. 215–216 (2013) 859–867.
[5] J. Goscianska, M. Ptaszkowska-Koniarz, M. Frankowski, M. Franus, R. Panek, W. Franus, Removal of phosphate from water by lanthanum-modified zeolites obtained from fly ash, J. Colloid Interface Sci. 513 (2018) 72–81.
[6] C. Yu, J. Geng, Y. Zhuang, J. Zhao, L. Chu, X. Luo, Y. Zhao, Y. Guo, Preparation of the chitosan grafted poly (quaternary ammonium)/Fe3O4 nanoparticles and its adsorption performance for food yellow 3, Carbohydr. Polym. 152 (2016) 327–336.
[7] Y. Huang, X. Lee, F.C. Macazo, M. Grattieri, R. Cai, S.D. Minteer, Fast and efficient removal of chromium (VI) anionic species by a reusable chitosan-modified multiwalled carbon nanotube composite, Chem. Eng. J. 339 (2018) 259–267.
[8] N. Li, R. Bai, A novel amine-shielded surface cross-linking of chitosan hydrogel beads for enhanced metal adsorption performance, Ind. Eng. Chem. Res. 44 (2005) 6692–6700.
[9] N. Li, R. Bai, Highly enhanced adsorption of lead ions on chitosan granules functionalized with poly (acrylic acid), Ind. Eng. Chem. Res. 45 (2006) 7897–7904.
[10] W.W. Ngah, S. Fatinathan, Pb (II) biosorption using chitosan and chitosan derivatives beads: Equilibrium, ion exchange and mechanism studies, J. Environ. Sci. 22 (2010) 338–346.
[11] T. Li, Y. Liu, S. Wang, G. Zeng, B. Zheng, H. Wang, M. Zhang, F. Guo, X. Zeng, Synthesis and adsorption application of amine shield-introduced-released porous chitosan hydrogel beads for removal of acid orange 7 from aqueous solutions, RSC Adv. 5 (2015) 62778–62787.
[12] L. Dong, C. Wen, Y. Junxia, D. Yigang, Polyamine chitosan adsorbent for the enhanced adsorption of anionic dyes from water, J. Dispersion Sci. Technol. 38 (2017) 1832–1841.
[13] N. Li, R. Bai, Development of chitosan-based granular adsorbents for enhanced and selective adsorption performance in heavy metal removal, Water Sci. Technol. A J. Int. Assoc. Water Pollut. Res. 54 (2006) 103–113.
[14] F. Haghseresht, S. Wang, D.D. Do, A novel lanthanum-modified bentonite, Phoslock, for phosphate removal from wastewaters, Appl. Clay Sci. 46 (2009) 369–375.
[15] Z. Wang, D. Shen, F. Shen, T. Li, Phosphate adsorption on lanthanum loaded biochar, Chemosphere 150 (2016) 1–7.
[16] P. Koilraj, K. Sasaki, Selective removal of phosphate using La-porous carbon composites from aqueous solutions: batch and column studies, Chem. Eng. J. 317 (2017)

1059–1068.
[17] S. Zhang, M. A.S. Abdalla, Z. Luo, S. Xia, The wheat straw biochar research on the adsorption/desorption behaviour of mercury in wastewater, 2018.
[18] X. Zhao, J. Wang, S. Wang, G. Xing, Successive straw biochar application as a strategy to sequester carbon and improve fertility: A pot experiment with two rice/wheat rotations in paddy soil, Plant Soil 378 (2014) 279–294.
[19] W.Y. Huang, D. Li, Z.Q. Liu, Q. Tao, Y. Zhu, J. Yang, Y.M. Zhang, Kinetics, isotherm, thermodynamic, and adsorption mechanism studies of La(OH) 3 -modified exfoliated vermiculites as highly efficient phosphate adsorbents, Chem. Eng. J. 236 (2014) 191–201.
[20] M.-M. Zhang, Y.-G. Liu, T.-T. Li, W.-H. Xu, B.-H. Zheng, X.-F. Tan, H. Wang, Y.-M. Guo, F.-Y. Guo, S.-F. Wang, Chitosan modification of magnetic biochar produced from Eichhornia crassipes for enhanced sorption of Cr (vi) from aqueous solution, RSC Adv. 5 (2015) 46955–46964.
[21] J. Deng, Y. Liu, S. Liu, G. Zeng, X. Tan, B. Huang, X. Tang, S. Wang, Q. Hua, Z. Yan, Competitive adsorption of Pb (II), Cd (II) and Cu (II) onto chitosan-pyromellitic dianhydride modified biochar, J. Colloid Interface Sci. 506 (2017) 355–364.
[22] M.Z. Afzal, X.-F. Sun, J. Liu, C. Song, S.-G. Wang, A. Javed, Enhancement of ciprofloxacin sorption on chitosan/biochar hydrogel beads, Sci. Total Environ. 639 (2018) 560–569.
[23] Q. Yang, F. Dou, B. Liang, Q. Shen, Studies of cross-linking reaction on chitosan fiber with glyoxal, Carbohydr. Polym. 59 (2005) 205–210.
[24] M. Ruiz, A.M. Sastre, E. Guibal, Palladium sorption on glutaraldehyde-crosslinked chitosan, React. Funct. Polym. 45 (2000) 155–173.
[25] A.M. Fekry, Study for the stability and corrosion inhibition of electrophoretic deposited chitosan on mild steel alloy in acidic medium, Int. J. Electrochem. Sci. 7 (2012) 7270.
[26] N.A. Travlou, G.Z. Kyzas, N.K. Lazaridis, E.A. Deliyanni, Functionalization of graphite oxide with magnetic chitosan for the preparation of a nanocomposite dye adsorbent, Langmuir 29 (2013) 1657–1668.
[27] S. Liu, B. Huang, L. Chai, Y. Liu, G. Zeng, X. Wang, W. Zeng, M. Shang, J. Deng, Z. Zhou, Enhancement of As(V) adsorption from aqueous solution by a magnetic chitosan/biochar composite, RSC Adv. 7 (2017) 10891–10900.
[28] H. Qiu, C. Liang, J. Yu, Q. Zhang, M. Song, F. Chen, Preferable phosphate sequestration by nano-La(III) (hydr)oxides modified wheat straw with excellent properties in regeneration, Chem. Eng. J. 315 (2017) 345–354.
[29] Y. He, H. Lin, Y. Dong, L. Wang, Preferable adsorption of phosphate using lanthanum-incorporated porous zeolite: characteristics and mechanism, Appl. Surf. Sci. 426 (2017) 995–1004.
[30] Y. Huang, X. Lee, M. Grattieri, F.C. Macazo, R. Cai, S.D. Minteer, A sustainable adsorbent for phosphate removal: modifying multi-walled carbon nanotubes with chitosan, J. Mater. Sci. 53 (2018) 12641–12649.
[31] J. Zhang, Z. Shen, W. Shan, Z. Mei, W. Wang, Adsorption behavior of phosphate on lanthanum (III)-coordinated diamino-functionalized 3D hybrid mesoporous silicates material, J. Hazard. Mater. 186 (2011) 76–83.
[32] L. Zhang, Q. Zhou, J. Liu, N. Chang, L. Wan, J. Chen, Phosphate adsorption on lanthanum hydroxide-doped activated carbon fiber, Chem. Eng. J. 185–186 (2012) 160–167.
[33] C.-J. Na, M.-J. Yoo, D.C. Tsang, H.W. Kim, K.-H. Kim, High-performance materials for effective sorptive removal of formaldehyde in air, J. Hazard. Mater. (2018).
[34] M. Nehra, N. Dilbaghi, N.K. Singhal, A.A. Hassan, K.-H. Kim, S. Kumar, Metal organic frameworks MIL-100 (Fe) as an efficient adsorptive material for phosphate management, Environ. Res. 169 (2019) 229–236.
[35] K. Vikrant, K.-H. Kim, Nanomaterials for the adsorptive treatment of Hg (II) ions from water, Chem. Eng. J. (2018).
[36] W. Xiong, J. Tong, Z. Yang, G. Zeng, Y. Zhou, D. Wang, P. Song, R. Xu, C. Zhang, M. Cheng, Adsorption of phosphate from aqueous solution using iron-zirconium modified activated carbon nanofiber: performance and mechanism, J. Colloid Interface Sci. 493 (2017) 17–23.
[37] X. Liu, L. Zhang, Removal of phosphate anions using the modified chitosan beads: adsorption kinetic, isotherm and mechanism studies, Powder Technol. 277 (2015) 112–119.
[38] Q. Xie, Y. Li, Z. Lv, H. Zhou, X. Yang, J. Chen, H. Guo, Effective adsorption and removal of phosphate from aqueous solutions and eutrophic water by Fe-based MOFs of MIL-101, Sci. Rep. 7 (2017) 3316.
[39] J. Ray, S. Jana, T. Tripathy, Synthesis of dipolar grafted hydroxyethyl cellulose and its application for the removal of phosphate ion from aqueous medium by adsorption, Int. J. Biol. Macromol. 109 (2018) 492–506.
[40] H. Fu, Y. Yang, R. Zhu, J. Liu, M. Usman, Q. Chen, H. He, Superior adsorption of phosphate by ferrihydrite-coated and lanthanum-decorated magnetite, J. Colloid Interface Sci. 530 (2018) 704–713.
[41] J. Wang, L. Zhao, W. Duan, L. Han, Y. Chen, Adsorption of Aqueous Cr(VI) by Novel Fibrous Adsorbent with Amino and Quaternary Ammonium Groups, Ind. Eng. Chem. Res. 51 (2012) 13655–13662.
[42] B. Wu, L. Fang, J.D. Fortner, X. Guan, I.M.C. Lo, Highly efficient and selective phosphate removal from wastewater by magnetically recoverable La(OH)3/Fe3O4 nanocomposites, Water Res. 126 (2017) 179–188.